

UnCLE: Unsupervised Continual Learning of Depth Completion

Suchisrit Gangopadhyay^{1*}, Xien Chen^{1*}, Michael Chu^{1*}, Patrick Rim¹, Hyoungseob Park¹, Alex Wong¹

I. ABSTRACT

We propose UnCLE, a standardized benchmark for Unsupervised Continual Learning of a multimodal depth estimation task: Depth completion aims to infer a dense depth map from a pair of synchronized RGB image and sparse depth map. We benchmark depth completion models under the practical scenario of unsupervised learning over continuous streams of data. Existing methods are typically trained on a static, or stationary, dataset. However, when adapting to novel non-stationary distributions, they “catastrophically forget” previously learned information. UnCLE simulates these non-stationary distributions by adapting depth completion models to sequences of datasets containing diverse scenes captured from distinct domains using different visual and range sensors. We adopt representative methods from continual learning paradigms and translate them to enable unsupervised continual learning of depth completion. We benchmark these models for indoor and outdoor and investigate the degree of catastrophic forgetting through standard quantitative metrics. Furthermore, we introduce model inversion quality as an additional measure of forgetting. We find that unsupervised continual learning of depth completion is an open problem, and we invite researchers to leverage UnCLE as a development platform.

II. INTRODUCTION

Three-dimensional (3D) perception is fundamental for spatial tasks such as autonomous navigation, robotic manipulation, and augmented reality. The systems to tackle these tasks are typically built upon a sensor suite including range (e.g. lidar, radar) and optics (e.g. camera). Depth completion is the task of recovering the dense depth map of a 3D scene from the measurements of these range sensors, which often yield sparse 3D coordinates, by leveraging the dense 2D topology captured in RGB images.

Despite these advantages, existing depth completion methods are predominately trained and tested on a single dataset under the assumption that the distribution of 3D scenes is stationary. When deployed in the real world with evolving conditions and unseen domains where the encountered distribution is non-stationary, the model must be continually trained to adapt to new scenes. However, continual re-training can lead to the problem of where a model’s performance degrades significantly on previously learned tasks when trained on new tasks [1], [2], [3], [4]. This problem is commonly referred to as “catastrophic forgetting.”

Continual (or lifelong) learning is the training paradigm that addresses the challenge of catastrophic forgetting by enabling a single model to learn from a continual non-stationary stream of datasets, adapting to new tasks while preserving performance on previous tasks. Retraining models for supervised 3D tasks on new domains is often impractical due to the difficulty and high cost of acquiring accurate ground-truth. This highlights the need for methods that can learn new data distributions in an unsupervised manner. Therefore, our work investigates unsupervised continual learning for depth completion, aiming to enable a multimodal depth estimation model to learn new domains without ground-truth while retaining performance on previously seen domains.

This paper presents a comprehensive benchmark for existing unsupervised continual learning methods for depth completion to streamline further research in this area. We begin with the motivating observation of how the performance of three unsupervised depth completion models [5], [6], [7] degrades after being finetuned on two sequences of datasets. We adopt three canonical continual learning methods (i.e., regularization-based [8], [9] and rehearsal-based [10] methods) for the 3D perception task of unsupervised depth completion. We evaluate on sequences of both indoor [11], [7], [12] and outdoor [13], [14], [15] datasets and detail our evaluation protocols for future methods.

Furthermore, we present model inversion as a new qualitative evaluation protocol to measure catastrophic forgetting of 3D vision models. Model inversion is the reconstruction of input data given the corresponding output and the frozen model weights. We can compare continual learning methods by evaluating the fidelity of reconstructed input data from previously seen domains using the weights trained on new tasks. This is based on the assumption that a model that can reconstruct the input image has experienced less forgetting.

Our contributions are as follows:

- We are the first to adapt existing, canonical regularization-based and rehearsal-based continual learning methods for unsupervised depth completion. After implementing these methods, we re-tune the existing best training settings for the depth completion models that we use for each continual learning method.
- We provide extensive quantitative results on a sequence of indoor datasets, and on another sequence of outdoor datasets. In this way, we demonstrate the effectiveness of continual learning methods for lifelong learning of tasks spanning from robotics to autonomous driving.
- We introduce model inversion, a novel qualitative evaluation protocol to measure catastrophic forgetting of 3D vision models.

*Equal contribution

¹Authors are with the Department of Computer Science, Yale University, CT 06520, USA, {firstname.lastname}@yale.edu

III. RELATED WORKS

A. Continual Learning

Regularization-based One approach to mitigating catastrophic forgetting is through regularization, which introduces constraints or penalties to the loss function to ensure that new tasks are learned without significantly altering the weights from previous training. The first class of methods in this category focuses on weight regularization, selectively constraining changes to network parameters that are important for previous tasks. Elastic Weight Consolidation (EWC) [8] selectively decreases the plasticity of model weights determined by the Fisher information matrix. [16] estimates parameter importance based on their contribution to loss changes during training. [17] assess importance by measuring the sensitivity of model outputs to parameter variations. [18] combines the regularization techniques of [8] and [16] to leverage their strengths in mitigating catastrophic forgetting.

The other class of regularization-based techniques focuses on function regularization, which aims to preserve the model’s output behavior on previous tasks by constraining changes in the intermediate features or final predictions through the knowledge distillation (KD) framework [19]. Learning Without Forgetting (LwF) [9] is a pioneering approach that mitigates catastrophic forgetting by using the new task data to approximate the responses of the old model. To further enhance retention, LwM [20] integrates attention maps into the KD process to capture essential feature representations, while EBLL [21] preserves feature reconstructions by utilizing task-specific autoencoders. Methods like GD [22] leverage external unlabeled data to extend regularization beyond the training set, increasing the model’s ability to generalize to unseen tasks. Generative approaches such as MeRGANs [23] and LifelongGAN [24] simulate old task data, thus reducing the need for storing large datasets. Additionally, feature-based regularization techniques like PODNet [25] and LUCIR [26] work to preserve feature similarity, addressing distribution shifts between tasks and improving overall stability. Bayesian approaches also offer robust function regularization. FRCL [27] and FROMP [28] use probabilistic models to regularize the functional space, providing smooth task transitions by quantifying uncertainty. Broader frameworks like VCL [29] extend these ideas, using variational inference to maintain a balance between task stability and plasticity. In this paper, we choose to concentrate on EWC and LWF as we find them to be milestone works of the two classes of regularization-based approaches.

Rehearsal-based Replay-based approaches in continual learning mitigate catastrophic forgetting by reintroducing past examples during the training of new tasks. These methods include Experience Replay (“Replay”) [10], which stores actual samples from previous tasks to train on again and reinforce performance on previously seen data. Within Experience Replay, there are different selection strategies for choosing the replay buffer, such as randomized Reservoir Sampling [30], [31], [32], class-based sampling [33], [34], and Generative replay [35] utilizes generative models like

GANs or VAEs to produce synthetic data mimicking the data distributions of previous tasks. Variational autoencoder approaches [36], [37], [38], [39], [40], [41] are able to control the generated data labels, but suffer from blurry quality. GAN approaches [42], [41], [43] are able to improve the quality of the generated input data over the VAE methods. Feature replay stores data on the feature-level instead of the raw input data in order to be less resource-expensive. Some approaches [44], [45], [46] use feature distillation between new and old models. [47] stores initial class statistics, like mean and covariance, to rectify biases in predictions. For our benchmark, we opt to use Experience Replay as our baseline for rehearsal-based continual learning methods as it is the foundation for rehearsal-based methods. Its direct use of actual training data, despite being resource-intensive, makes it a more effective method, especially crucial for the high fidelity required in unsupervised depth completion tasks. We use randomized sampling because many of the other discussed sampling methods are either specific to classification tasks or have similar performance.

Token-based These methods aim to store information learned from previous tasks in a small, fixed set of weights called “tokens,” which can be thought of as learnable biases. Some methods additionally utilize a small memory buffer, but others are able to obtain similar performance without one. They are often cheap and scalable, and recent methods have achieved state-of-the-art results in continual learning for image classification. However, these methods are currently for 2D classification tasks [48], [49], [50] or can only be applied to transformer-based architectures [51]. Token-based continual learning methods for 3D regression tasks, such as depth completion, have not yet been explored. Thus, we are not able to obtain baselines for these methods for depth completion.

Continual Learning for Depth Estimation The MonoDepthCL [51] framework, employs a dual-memory rehearsal-based method to address the challenges of catastrophic forgetting in unsupervised monocular depth estimation. CoDEPS [52] employs a unique domain-mixing strategy for pseudo-label generation with efficient experience replay. However, previous works in this field typically focus on a single modality and lack standardized benchmarks, limiting their applicability to real-world scenarios where the use of multi-modal data is standard. Our paper contributes to this field by establishing a benchmark for depth completion using both images and sparse depth data, addressing these gaps and setting a foundation for future research in continual depth estimation.

B. Depth Completion

Depth estimation is the task of reconstructing the 3D scene from visual inputs, e.g., a pair of calibrated stereo images [53], [54], [55], [56] or a monocular image [57], [57], [58], [59], [60], [61], [62], [63], [64]. Inferring depth from a single image is an ill-posed task; recovering metric depth typically requires an additional sensor, e.g., lidar [65], [66], radar [67].

Depth completion [68], [69], [70], [71] is the task of inferring a dense metric depth from an RGB image and synchronized sparse point cloud. Supervised methods [72], [73], [74], [75], [76], [77], [78], [79] rely on large datasets with ground-truth dense depth maps, which are used to train models capable of mapping sparse depth points and RGB images to dense depth maps. While effective, these approaches are limited by the availability and cost of obtaining annotated data, making it less practical for continual learning scenarios where the collection of new data may not include dense depth map annotations. Supervised depth completion methods are less practical than unsupervised approaches, as achieving precise dense depth maps for every task in a continual learning scenario is challenging.

Unsupervised depth completion methods [80], [81], [7], [6], [82], [83], [68], [70], in contrast, leverage the inherent structure and patterns within the RGB image and sparse depth data to infer missing depth values, making them more adaptable for continual learning as they do not require dense ground-truth depth maps. [80] utilized Perspective-n-Point [84] and RANSAC [85] to align adjacent video frames. [68] trains a depth prior constrained on the image. FusionNet [6] leverages synthetic data to learn a prior from a scene, while [86] converts synthetic data to real domain to use rendered depth. VOICED [7] approximated a scene with scaffolding. [82] introduced an adaptive scheme to reduce penalties incurred on occluded regions. KBNet [5] maps the image onto the 3D scene frustum using calibrated back-projection. [83] decouples scale and structure. [87] uses visual SLAM features and [69] proposed monitored distillation for positive congruent training.

However, all of these methods are subject to catastrophic forgetting as they rely on updating model weights to fit onto a new target dataset without the objective of retaining past information. This aspect makes it challenging for them to adapt to a continual learning setting where both new and previously seen tasks need to be handled without performance degradation on either. Therefore, it is critical to develop methods for these models that enable continual learning, ensuring that they can effectively adapt to new data while preserving previous examples.

IV. METHOD FORMULATION

Problem definition. The task of unsupervised depth completion can be formulated as follows: Let $I : \Omega \subset \mathbb{R}^2 \rightarrow \mathbb{R}_+^3$ denote an RGB image at current timestamp t obtained from a calibrated camera, and $z : \Omega_z \subset \Omega \rightarrow \mathbb{R}_+$ represent the corresponding sparse depth map derived from a projected 3D point cloud. Given the image I , the sparse depth map z , and the intrinsic calibration matrix $K \in \mathbb{R}^{3 \times 3}$, the goal is to learn a function $f_\theta(I, z)$ that estimates a dense depth map, which accurately recovers the distances between the camera and all visible points in the 3D scene, without relying on ground-truth depth annotations. Similarly to [5], instead of using ground truth we use a photometric reprojection error by comparing the reconstructed image I_t from adjacent frames I_τ for $\tau \in \{t-1, t+1\}$ with the estimated relative camera

pose matrix $g_{\tau t} \in SE(3)$. To estimate $g_{\tau t}$, we jointly train a pose network $p_\theta(I, I_\tau)$:

$$\hat{I}_\tau(x, \hat{d}, g_{\tau t}) = I_\tau(\pi g_{\tau t} K^{-1} \bar{x} \hat{d}(x)). \quad (1)$$

In this formula, K is the camera's intrinsic matrix, π is the canonical perspective projection, and \bar{x} represents the homogeneous coordinates $[x^\top, 1]^\top$ of $x \in \Omega$. We train $p_\theta(I, I_\tau)$ during training-time, but it is not used for inference.

In the continual learning setting, our objective is to adapt a pretrained model f_θ and p_θ , trained on an initial dataset $T_0 = \{(I_0^{(i)}, z_0^{(i)}, K_0^{(i)})\}_{i=1}^n$, to a sequence of new datasets T_1, T_2, \dots, T_N , where each $T_k = \{(I_k^{(i)}, z_k^{(i)}, K_k^{(i)})\}_{i=1}^{n_k}$ and n_k denotes the number of training examples in T_k . The challenge is to incrementally train both f_θ and p_θ on each new target dataset T_k without experiencing significant degradation in performance on the source dataset S and all previously seen target datasets $T_j \forall j < k$. This requires effectively mitigating catastrophic forgetting while enabling the model to generalize across different domains in the depth completion task.

Unsupervised Depth Completion Loss. We train $f_\theta(I, z)$ to minimize

$$\mathcal{L} = w_{ph} \ell_{ph} + w_{sz} \ell_{sz} + w_{sm} \ell_{sm} \quad (2)$$

where each loss term can be weighted differently by their respective w .

The photometric consistency loss,

$$\ell_{ph} = \frac{1}{|\Omega|} \sum_{\tau \in T} \sum_{x \in \Omega} w_{co} |\hat{I}_\tau(x) - I(x)| + w_{st} (1 - \text{SSIM}(\hat{I}_\tau(x), I(x))), \quad (3)$$

encourages both structural and color similarity between the reconstructed and actual center images.

The sparse depth consistency loss,

$$\ell_{sz} = \frac{1}{|\Omega_z|} \sum_{x \in \Omega_z} |\hat{d}(x) - z(x)|. \quad (4)$$

encourages consistency between the input sparse depth and predicted depth map over the sparse depth map's domain (Ω_z).

The local smoothness loss,

$$\ell_{sm} = \frac{1}{|\Omega|} \sum_{x \in \Omega} \lambda_X(x) |\partial_X \hat{d}(x)| + \lambda_Y(x) |\partial_Y \hat{d}(x)|. \quad (5)$$

encourages local smoothness by penalizing depth map gradients in the x - (∂_X) and y - (∂_Y) directions. These gradients are weighted by the corresponding image gradients $\lambda_X = e^{-|\partial_X I_t(x)|}$ and $\lambda_Y = e^{-|\partial_Y I_t(x)|}$ to account for object edges.

A. Elastic Weight Consolidation

For the task of continual depth completion, we implement EWC as follows. When training on a new dataset T_k , we first load the previously trained model f_{θ^*} , which is parameterized by the weight matrices θ^* optimized for T_{k-1} . These parameters are frozen and treated as a reference during

training on T_k . The Fisher information matrix F_i quantifies each parameter's θ_i importance to the previous model's performance on T_{k-1} . The final EWC loss is therefore defined as:

$$\mathcal{L}_{\text{ewc}} = \lambda_{\text{ewc}} \sum_i \frac{1}{2} F_i (\theta_i - \theta_i^*)^2 \quad (6)$$

EWC loss penalizes important weights from moving too far away from their values optimized for the previous task. We add this to the total loss for unsupervised depth completion \mathcal{L} in Eq. 2 with $\lambda_{\text{ewc}} = 1$, which we found to be optimal after extensive tuning.

B. Learning Without Forgetting

To implement Learning Without Forgetting (LwF) for the depth completion task, we aim to preserve output behavior from previous tasks while training only on new data. Specifically, we load the checkpoint of the old model f_θ , which are kept frozen during training. This old model processes the new data to generate predictions, denoted as $\hat{I}_\tau(x, \hat{d}, g_{\tau t})$, where \hat{d} represents the predicted depth and $g_{\tau t}$ is the relative pose transformation between frames.

We compute a mean squared error (MSE) loss between the outputs of the frozen model and the new model f'_θ . This LwF loss encourages the new model's predictions $\hat{I}'_\tau(x, \hat{d}, g_{\tau t})$ to remain consistent with the frozen model's predictions. Simultaneously, the joint loss function \mathcal{L}_{lwf} includes the loss between the new model's output and the ground truth depth data from the current task. The final loss function is defined as:

$$\mathcal{L}_{\text{lwf}} = \lambda_o \cdot \mathcal{L}_{\text{old}} + \mathcal{L}_{\text{new}} \quad (7)$$

Here, \mathcal{L}_{old} computes the loss between the frozen model's output \hat{I}_τ and the new model's output \hat{I}'_τ , while \mathcal{L}_{new} is the loss between the new model's output I_n and the ground truth depth map z_n . Both \mathcal{L}_{old} and \mathcal{L}_{new} include all the terms in the unsupervised loss algorithm \mathcal{L} in Eq. 2. The parameter λ_o balances the contribution of the old and new task losses. After many experiments, we set the optimal λ_o to be 0.5.

This approach allows the model to learn from new depth data without requiring access to previous task data, as the frozen model's predictions act as a proxy for past knowledge.

C. Experience Replay

To perform experience replay with depth completion, we maintain a replay buffer, which retains a fixed number of representative samples from each dataset previously trained on. The selections and the integration of the replay buffer into the new task are designed to balance computational efficiency with performance retention. Empirically, a buffer size of 64 data points for each previous dataset was determined to offer an optimal balance. During each training iteration on a new target dataset, a batch of data from the replay buffer is reintroduced into the training process. The data points from both the current and historical datasets are processed as follows:

Let $\mathcal{D}_{\text{new}} = T_k$ denote the set of new training data points from the current target dataset, where N is the number of new data points. Similarly, let $\mathcal{D}_{\text{replay}} = \{(I_r^{(j)}, z_r^{(j)}, K_r^{(j)})\}_{j=1}^M$ denote the set of replayed data points from the buffer, where M is the number of data points in the replay buffer. Each training batch is made up of a 50-50 new-replay data ratio, where the replay half is evenly split between previous datasets. The total loss function $\mathcal{L}_{\text{total}}$ for a training iteration is then formulated as:

$$\mathcal{L}_{\text{total}} = \mathcal{L}_{\text{new}} + \mathcal{L}_{\text{replay}} \quad (8)$$

where \mathcal{L}_{new} is the unsupervised loss \mathcal{L} in Eq. 2 computed on the new training data, and $\mathcal{L}_{\text{replay}}$ is the unsupervised loss \mathcal{L} computed on the replayed data.

During training, the loss $\mathcal{L}_{\text{replay}}$ computed from the data points in the replay buffer is equal to total loss $\mathcal{L}_{\text{total}}$ from the preceding continual training step, ensuring consistency and retention of previously acquired knowledge.

D. Model Inversion

We propose a method of using model inversion to evaluate a model's forgetting. In other words, we can try to retrieve an image that a model $f_\omega(I, z)$ was trained on using just its weights and a supervised output complete depth map d . To invert a depth completion model, we freeze the model, start with a uniformly random set of pixels \tilde{I} , and update \tilde{I} to minimize $\|f_\theta(\tilde{I}, z) - d\|_1$, where z is the data point's actual sparse depth map. To evaluate the model's forgetting we use the pretrained model $f_\theta(I, z)$ to get $d = f_\theta(I, z)$, where I and z are the actual input image and sparse depth for the data point. Thus, we ultimately minimize $\|f_\omega(\tilde{I}, z) - f_\theta(I, z)\|_1$ to retrieve an old training image from $f_\omega(I, z)$, having been trained on new data. Although we try to retrieve a trained image, a similar method can be used to retrieve the input sparse depth map.

V. EXPERIMENTS

For evaluation, we compute four key metrics: Mean Absolute Error (MAE), Root Mean Squared Error (RMSE), Inverse MAE (iMAE), and Inverse RMSE (iRMSE). These metrics are described in detail in Table XIV. For qualitative results, we use the proposed model inversion method to measure catastrophic forgetting on the previous task dataset. Our experiments consist of continual training on both indoor and outdoor datasets. For indoor sequences, we first train on NYUv2 (Table I) and evaluate the continual learning process over the sequences NYUv2 \rightarrow ScanNet \rightarrow VOID (Tables II, III, and IV), and NYUv2 \rightarrow VOID \rightarrow ScanNet (Tables V, VI, and VII). For outdoor sequences, we train on KITTI and evaluate on KITTI \rightarrow Virtual KITTI \rightarrow Waymo (Tables VIII, IX, and X), and KITTI \rightarrow Waymo \rightarrow Virtual KITTI (Tables XI, XII, and XIII).

A. Datasets

We use three datasets for indoor experiments and three datasets for outdoor experiments. *Indoor datasets:* The **NYU Depth V2** dataset [11] contains 464 indoor scenes captured

TABLE I: Performance of the pretrained models on the NYUv2 (initial indoor) and KITTI (initial outdoor) datasets.

Model	NYUv2				KITTI			
	MAE ↓	RMSE ↓	iMAE ↓	iRMSE ↓	MAE ↓	RMSE ↓	iMAE ↓	iRMSE ↓
VOICED	94.641	177.134	18.492	39.309	295.410	1159.270	1.200	3.490
FusionNet	102.872	192.23	20.913	42.821	267.690	1157.070	1.080	3.190
KBNet	85.842	169.833	17.065	35.368	256.961	1122.597	1.011	3.155

TABLE II: *Evaluation on NYUv2*. Starting from NYUv2 pretrained weights, models are trained on ScanNet (NYUv2 → ScanNet) and subsequently on VOID (NYUv2 → ScanNet → VOID)

Model	Method	NYUv2 → ScanNet				NYUv2 → ScanNet → VOID			
		MAE ↓	RMSE ↓	iMAE ↓	iRMSE ↓	MAE ↓	RMSE ↓	iMAE ↓	iRMSE ↓
VOICED	Finetuned	102.556	193.830	19.794	44.300	105.918	193.336	19.977	42.623
	EWC	99.426	188.504	19.866	45.909	111.247	205.710	19.425	39.442
	LwF	106.500	198.029	24.327	64.434	111.632	200.986	19.580	40.796
	Replay	101.879	187.149	20.214	43.836	104.386	187.938	21.597	45.943
FusionNet	Finetuned	106.999	202.943	20.984	43.806	117.709	205.254	21.647	40.639
	EWC	113.555	217.060	23.441	50.584	107.319	201.506	19.765	39.049
	LwF	100.577	188.393	18.645	36.827	103.157	192.620	18.413	35.504
	Replay	102.422	193.054	20.908	43.278	100.180	187.368	19.583	39.493
KBNet	Finetuned	94.357	193.184	17.321	38.087	108.699	215.057	19.139	40.711
	EWC	90.145	186.402	16.529	36.180	102.277	200.576	17.945	37.814
	LwF	97.987	186.385	18.598	38.178	91.784	177.807	17.628	37.366
	Replay	91.243	175.683	18.957	39.680	95.622	184.347	19.312	40.620

TABLE III: *Evaluation on ScanNet*. Starting from NYUv2 pretrained weights, models are trained on ScanNet (NYUv2 → ScanNet) and subsequently on VOID (NYUv2 → ScanNet → VOID)

Model	Method	NYUv2 → ScanNet				NYUv2 → ScanNet → VOID			
		MAE ↓	RMSE ↓	iMAE ↓	iRMSE ↓	MAE ↓	RMSE ↓	iMAE ↓	iRMSE ↓
VOICED	Finetuned	19.077	47.153	7.421	18.953	20.261	47.069	7.850	18.953
	EWC	18.496	46.451	7.155	18.673	19.553	47.143	7.375	18.933
	LwF	20.715	47.719	8.105	19.566	19.739	47.770	7.408	19.101
	Replay	21.478	52.750	7.681	19.395	21.711	53.581	7.544	19.417
FusionNet	Finetuned	18.021	48.733	6.520	18.896	25.064	52.576	9.898	21.274
	EWC	17.756	47.644	6.521	18.874	17.943	47.301	9.689	19.085
	LwF	16.231	44.917	5.986	17.924	17.349	45.771	6.517	18.304
	Replay	17.352	48.241	5.909	17.841	18.149	49.309	6.128	17.923
KBNet	Finetuned	14.290	41.550	5.289	16.610	15.961	44.048	5.866	17.393
	EWC	14.091	41.344	5.230	16.578	16.992	44.559	6.756	17.856
	LwF	16.060	43.786	5.675	16.748	17.358	45.771	6.028	17.111
	Replay	14.690	42.702	5.100	16.192	15.265	43.755	5.721	16.447

TABLE IV: *Evaluation on VOID*. Starting from NYUv2 pretrained weights, models are trained on ScanNet (NYUv2 → ScanNet) and subsequently on VOID (NYUv2 → ScanNet → VOID)

Model	Method	NYUv2 → ScanNet → VOID			
		MAE ↓	RMSE ↓	iMAE ↓	iRMSE ↓
VOICED	Finetuned	37.656	93.155	19.229	46.179
	EWC	39.356	95.292	19.058	43.938
	LwF	37.585	90.167	19.413	44.805
	Replay	42.275	100.427	21.953	49.866
FusionNet	Finetuned	36.010	87.008	18.540	43.159
	EWC	35.195	87.492	17.600	42.119
	LwF	34.572	85.400	17.499	41.203
	Replay	35.363	91.210	18.582	45.632
KBNet	Finetuned	32.313	83.962	16.163	40.282
	EWC	35.139	89.733	18.923	45.515
	LwF	36.032	90.976	19.718	48.217
	Replay	34.583	90.770	18.192	45.739

TABLE V: *Evaluation on NYUv2*. Starting from NYUv2 pretrained weights, models are trained on VOID (NYUv2 \rightarrow VOID) and subsequently on ScanNet (NYUv2 \rightarrow VOID \rightarrow ScanNet)

Model	Method	NYUv2 \rightarrow VOID				NYUv2 \rightarrow VOID \rightarrow ScanNet			
		MAE \downarrow	RMSE \downarrow	iMAE \downarrow	iRMSE \downarrow	MAE \downarrow	RMSE \downarrow	iMAE \downarrow	iRMSE \downarrow
VOICED	Finetuned	99.042	182.196	18.819	38.632	99.281	190.244	19.317	43.954
	EWC	106.489	193.701	19.039	38.042	100.611	192.186	20.232	47.167
	LwF	104.732	188.505	20.060	44.116	100.974	189.749	20.457	44.925
	Replay	103.689	190.762	20.651	43.913	103.848	189.240	22.354	48.550
FusionNet	Finetuned	103.278	193.581	19.207	38.495	108.858	208.497	22.423	48.256
	EWC	103.478	193.886	18.983	37.579	107.600	206.906	22.223	48.358
	LwF	100.143	186.084	18.301	35.863	95.975	180.125	17.545	34.595
	Replay	102.832	191.146	20.288	40.693	99.377	186.812	19.513	39.477
KBNet	Finetuned	122.475	241.367	21.239	45.710	94.590	194.518	17.170	37.546
	EWC	107.250	215.432	19.176	41.068	91.339	188.499	16.640	36.704
	LwF	105.551	186.658	21.038	44.658	88.545	174.485	17.333	36.729
	Replay	88.359	172.586	17.765	37.798	90.553	175.286	18.522	38.949

TABLE VI: *Evaluation on VOID*. Starting from NYUv2 pretrained weights, models are trained on VOID (NYUv2 \rightarrow VOID) and subsequently on ScanNet (NYUv2 \rightarrow VOID \rightarrow ScanNet)

Model	Method	NYUv2 \rightarrow VOID				NYUv2 \rightarrow VOID \rightarrow ScanNet			
		MAE \downarrow	RMSE \downarrow	iMAE \downarrow	iRMSE \downarrow	MAE \downarrow	RMSE \downarrow	iMAE \downarrow	iRMSE \downarrow
VOICED	Finetuned	38.963	93.236	20.730	47.662	38.825	90.594	22.433	50.817
	EWC	38.771	93.812	20.367	47.073	38.763	91.593	22.709	51.732
	LwF	42.499	97.798	24.867	56.016	45.398	100.679	28.677	60.894
	Replay	48.855	111.550	26.400	57.079	50.553	111.130	33.331	72.056
FusionNet	Finetuned	35.221	87.667	18.149	43.783	34.371	85.641	17.435	41.743
	EWC	35.446	87.978	18.158	42.460	36.762	93.557	20.917	54.146
	LwF	34.572	85.400	17.499	41.203	32.425	82.813	15.834	38.576
	Replay	36.542	91.689	19.489	46.890	37.752	94.848	21.040	51.004
KBNet	Finetuned	32.746	84.514	16.277	40.223	34.129	86.748	18.148	44.097
	EWC	34.572	86.971	17.827	43.114	34.643	89.025	18.807	46.172
	LwF	36.321	91.587	20.385	49.752	38.944	96.792	22.951	54.977
	Replay	34.544	90.054	18.392	45.751	39.409	99.833	21.509	52.007

TABLE VII: *Evaluation on ScanNet*. Starting from NYUv2 pretrained weights, models are trained on VOID (NYUv2 \rightarrow VOID) and subsequently on ScanNet (NYUv2 \rightarrow VOID \rightarrow ScanNet)

Model	Method	NYUv2 \rightarrow VOID \rightarrow ScanNet			
		MAE \downarrow	RMSE \downarrow	iMAE \downarrow	iRMSE \downarrow
VOICED	Finetuned	18.921	47.969	7.260	19.078
	EWC	18.584	47.835	7.302	19.397
	LwF	20.229	47.214	7.468	18.396
	Replay	25.125	55.480	9.297	20.723
FusionNet	Finetuned	16.889	47.318	6.170	18.574
	EWC	16.681	46.848	6.185	18.627
	LwF	16.192	44.808	5.937	17.789
	Replay	17.392	47.919	6.017	17.799
KBNet	Finetuned	14.070	41.372	5.169	16.390
	EWC	14.710	42.201	5.422	16.767
	LwF	15.578	42.373	5.428	16.112
	Replay	15.122	42.934	5.356	16.431

using RGB-D sensors, offering 1449 densely labeled pairs of aligned RGB and depth images. It is a benchmark dataset widely used in indoor depth estimation tasks. NYUv2 is the primary dataset on which we pretrain our depth completion models before outdoor continual learning. The **VOID** dataset [7] provides sparse depth maps and RGB frames for indoor environments, with approximately 58,000 frames. VOID emphasizes handling low-texture regions and scenes with

significant camera motion, which are crucial for testing robustness in indoor depth completion. **ScanNet** [12] is a large-scale indoor dataset that includes more than 2.5 million frames with corresponding RGB-D data. It provides dense depth ground truth and 3D reconstructions of indoor environments.

For the indoor datasets, we use the evaluation protocol in [7] and cap the depth values from 0.2 to 5 meters. During

TABLE VIII: *Evaluation on KITTI*. Starting from KITTI pretrained weights, models are trained on VKITTI (KITTI \rightarrow VKITTI) and subsequently on Waymo (KITTI \rightarrow VKITTI \rightarrow Waymo)

Model	Method	KITTI \rightarrow VKITTI				KITTI \rightarrow VKITTI \rightarrow Waymo			
		MAE \downarrow	RMSE \downarrow	iMAE \downarrow	iRMSE \downarrow	MAE \downarrow	RMSE \downarrow	iMAE \downarrow	iRMSE \downarrow
VOICED	Finetuned	345.655	1278.237	1.431	4.054	2327.250	3859.149	6.375	8.733
	EWC	353.852	1295.422	1.487	4.202	2625.052	4150.911	7.281	9.161
	LwF	414.647	1337.016	1.656	4.666	1801.192	3085.398	4.909	6.807
	Replay	351.029	1353.348	1.379	3.759	326.585	1344.943	1.247	3.715
FusionNet	Finetuned	281.757	1270.535	1.136	3.715	317.543	1281.393	1.274	3.697
	EWC	285.263	1285.849	1.139	3.715	284.831	1298.388	1.117	3.664
	LwF	277.504	1182.062	1.147	3.527	312.728	1221.368	1.403	3.945
	Replay	290.409	1310.964	1.106	3.537	293.817	1332.329	1.102	3.576
KBNet	Finetuned	311.888	1270.047	1.353	3.943	297.905	1252.206	1.222	3.655
	EWC	286.406	1266.132	1.127	3.667	315.838	1380.112	1.275	3.760
	LwF	277.309	1166.711	1.117	3.480	304.141	1184.546	1.531	4.204
	Replay	299.883	1368.686	1.082	3.473	307.247	1416.628	1.080	3.512

TABLE IX: *Evaluation on VKITTI*. Starting from KITTI pretrained weights, models are trained on VKITTI (KITTI \rightarrow VKITTI) and subsequently on Waymo (KITTI \rightarrow VKITTI \rightarrow Waymo)

Model	Method	KITTI \rightarrow VKITTI				KITTI \rightarrow VKITTI \rightarrow Waymo			
		MAE \downarrow	RMSE \downarrow	iMAE \downarrow	iRMSE \downarrow	MAE \downarrow	RMSE \downarrow	iMAE \downarrow	iRMSE \downarrow
VOICED	Finetuned	966.268	4031.375	1.295	3.449	7896.476	14200.599	9.852	13.761
	EWC	858.869	3881.263	1.142	3.242	5801.778	10616.265	7.568	10.538
	LwF	881.591	4055.195	1.215	3.403	5001.189	9463.238	6.963	10.024
	Replay	934.656	4153.693	1.066	2.866	1050.157	4211.335	1.734	3.228
FusionNet	Finetuned	631.225	3334.405	0.723	3.118	790.000	3685.247	1.153	3.782
	EWC	635.105	3365.572	0.666	2.917	787.348	3540.777	1.309	4.081
	LwF	612.924	3182.058	0.699	3.009	517.690	1667.856	1.236	2.685
	Replay	633.858	3348.971	0.596	2.692	645.891	3328.864	0.678	2.703
KBNet	Finetuned	658.075	3380.623	1.194	3.793	804.278	3759.132	1.155	3.856
	EWC	673.121	3552.306	0.872	3.373	814.097	3819.788	1.392	4.260
	LwF	741.125	3564.760	1.146	4.120	875.343	3681.855	2.778	6.438
	Replay	677.493	3567.431	0.854	3.452	714.782	3718.890	0.930	3.400

TABLE X: *Evaluation on Waymo*. Starting from KITTI pretrained weights, models are trained on VKITTI (KITTI \rightarrow VKITTI) and subsequently on Waymo (KITTI \rightarrow VKITTI \rightarrow Waymo)

Model	Method	KITTI \rightarrow VKITTI \rightarrow Waymo			
		MAE \downarrow	RMSE \downarrow	iMAE \downarrow	iRMSE \downarrow
VOICED	Finetuned	532.430	1731.000	1.216	2.656
	EWC	570.878	1770.593	1.272	2.724
	LwF	565.197	1758.846	1.280	2.719
	Replay	546.847	1756.500	1.199	2.586
FusionNet	Finetuned	535.436	1763.895	1.189	2.627
	EWC	496.805	1652.860	1.179	2.637
	LwF	633.107	3182.974	0.976	3.727
	Replay	486.746	1665.689	1.172	2.645
KBNet	Finetuned	485.462	1675.315	1.176	2.675
	EWC	480.940	1648.952	1.166	2.638
	LwF	522.286	1736.891	1.270	2.773
	Replay	497.199	1743.683	1.178	2.683

training, we use a crop shape of 416×576 for NYUv2 and a crop shape of 416×512 for VOID and Scannet.

Outdoor datasets: The **KITTI** dataset [13] is a widely used benchmark for autonomous driving, consisting of over 93,000 stereo image pairs and sparse LiDAR depth maps synchronized with the images that were captured from a wider range of urban and rural scenes. KITTI is the primary dataset on which we pretrain our depth completion models before

outdoor continual learning. The **Waymo** [14] Open Dataset includes approximately 230,000 frames of high-resolution images and dense LiDAR point clouds, covering a wide range of driving environments and conditions. **Virtual KITTI** [15] is a synthetic dataset designed to replicate KITTI scenes, providing over 21,000 frames with dense ground truth depth. It allows for evaluating domain adaptation, as we use multiple data domains to simulate domain discrepancies which cause

TABLE XI: *Evaluation on KITTI*. Starting from KITTI pretrained weights, models are trained on Waymo (KITTI → Waymo) and subsequently on VKITTI (KITTI → Waymo → VKITTI)

Model	Method	KITTI → Waymo				KITTI → Waymo → VKITTI			
		MAE ↓	RMSE ↓	iMAE ↓	iRMSE ↓	MAE ↓	RMSE ↓	iMAE ↓	iRMSE ↓
VOICED	Finetuned	1418.898	2543.668	4.608	7.031	388.247	1355.323	1.525	4.340
	EWC	1215.182	2238.520	4.056	6.447	442.459	1468.315	1.735	4.799
	LwF	2144.099	3518.483	5.767	7.693	415.244	1346.477	1.704	4.616
	Replay	337.384	1216.277	1.397	3.670	375.981	1216.501	1.512	3.800
FusionNet	Finetuned	322.472	1300.640	1.431	4.086	300.817	1298.835	1.288	4.011
	EWC	315.959	1273.695	1.292	3.823	379.437	1326.112	1.517	4.052
	LwF	296.444	1206.908	1.191	3.414	292.372	1208.645	1.214	3.661
	Replay	291.101	1310.897	1.094	3.493	302.014	1369.085	1.120	3.542
KBNet	Finetuned	351.044	1292.620	2.129	5.190	314.624	1273.683	1.480	4.225
	EWC	320.521	1282.303	1.499	4.256	305.615	1140.672	1.299	3.635
	LwF	291.704	1131.483	1.298	3.419	333.231	1228.935	1.874	4.548
	Replay	307.389	1413.860	1.082	3.478	353.075	1634.394	1.101	3.485

TABLE XII: *Evaluation on Waymo*. Starting from KITTI pretrained weights, models are trained on Waymo (KITTI → Waymo) and subsequently on VKITTI (KITTI → Waymo → VKITTI)

Model	Method	KITTI → Waymo				KITTI → Waymo → VKITTI			
		MAE ↓	RMSE ↓	iMAE ↓	iRMSE ↓	MAE ↓	RMSE ↓	iMAE ↓	iRMSE ↓
VOICED	Finetuned	525.367	1706.168	1.223	2.672	6236.390	7681.729	14.570	16.039
	EWC	525.354	1684.696	1.232	2.672	7389.857	9277.607	17.713	19.281
	LwF	565.813	1777.017	1.280	2.750	7508.272	9683.822	16.030	17.836
	Replay	583.101	1731.286	1.308	2.756	642.807	1771.024	1.407	2.822
FusionNet	Finetuned	512.323	1760.833	1.203	2.704	518.302	1772.169	1.210	2.708
	EWC	480.053	1637.659	1.166	2.627	495.613	1748.918	1.180	2.699
	LwF	469.060	1613.890	1.154	2.622	506.399	1644.618	1.210	2.665
	Replay	492.232	1685.874	1.149	2.565	508.490	1715.932	1.187	2.652
KBNet	Finetuned	496.915	1701.736	1.190	2.654	608.243	2144.506	1.213	2.699
	EWC	489.191	1709.312	1.180	2.696	620.688	1878.749	1.339	2.881
	LwF	493.037	1744.968	1.188	2.714	593.374	1777.834	1.387	2.913
	Replay	487.310	1704.594	1.170	2.664	581.065	1983.698	1.207	2.694

TABLE XIII: *Evaluation on VKITTI*. Starting from KITTI pretrained weights, models are trained on Waymo (KITTI → Waymo) and subsequently on VKITTI (KITTI → Waymo → VKITTI)

Model	Method	KITTI → Waymo → VKITTI			
		MAE ↓	RMSE ↓	iMAE ↓	iRMSE ↓
VOICED	Finetuned	858.263	3986.613	1.111	3.289
	EWC	909.536	4247.935	1.005	3.423
	LwF	914.993	4191.131	1.216	3.501
	Replay	910.002	4161.021	1.172	3.613
FusionNet	Finetuned	704.775	3421.726	0.947	5.643
	EWC	649.886	3419.303	0.631	2.697
	LwF	633.432	3199.120	0.935	3.826
	Replay	652.735	3407.310	0.631	2.748
KBNet	Finetuned	790.162	4124.413	1.004	4.177
	EWC	747.993	3706.933	0.999	3.301
	LwF	792.276	3492.584	1.416	4.583
	Replay	743.578	3754.860	1.038	3.741

catastrophic forgetting.

For KITTI and VKITTI, we cap the depth output during evaluation from 0.001 to 100 meters and use a depth crop of 240×1216 . During training, we use a crop of 320×768 . For Waymo, we cap the evaluation output from 0.001 to 80 meters and use a depth crop of 768×1920 , and we use a training crop of 800×640 .

B. Results

Quantitative. Observing the quantitative results, we see that the continual learning methods we use perform similarly well across datasets and depth completion models. According to Tables V and II, for indoor experiments, EWC outperforms the finetuned baseline by 1.6% on MAE and 0.71% on RMSE. LwF outperforms the finetuned model by 4% on MAE and 6.3% on RMSE. Replay outperforms the finetuned by 5.7% on

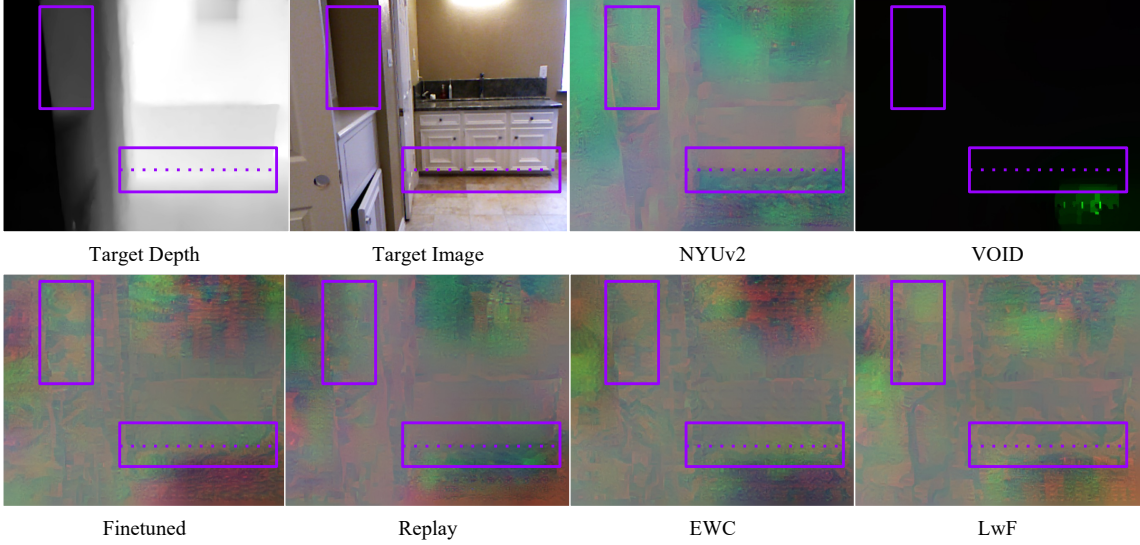


Fig. 1: **Model Inversion Qualitative Results** (Top row) We have the target image I we retrieve from the NYUv2 dataset and the target depth map predicted by inputting the image and its corresponding depth map into the KBnet NYUv2 pretrained model. We show an attempt at retrieving this image from the pretrained model and the VOID pretrained model for comparison. (Bottom) We also have the image retrieval attempts for KBnet models trained from NYUv2 to VOID with all of our continual learning methods.

Metric	Definition
MAE	$\frac{1}{ \Omega } \sum_{x \in \Omega} \hat{d}(x) - d_{gt}(x) $
RMSE	$(\frac{1}{ \Omega } \sum_{x \in \Omega} \hat{d}(x) - d_{gt}(x) ^2)^{1/2}$
iMAE	$\frac{1}{ \Omega } \sum_{x \in \Omega} 1/\hat{d}(x) - 1/d_{gt}(x) $
iRMSE	$(\frac{1}{ \Omega } \sum_{x \in \Omega} 1/\hat{d}(x) - 1/d_{gt}(x) ^2)^{1/2}$

TABLE XIV: *Error metrics.* d_{gt} denotes the ground-truth depth.

MAE and 7.4% on RMSE. According to Tables VIII and XI, for outdoor experiments, different from indoor experiments, regularization based continual learning methods harms the performance, where EWC performs worse than finetuning by 3.4% on MAE and 1% on RMSE. LwF performs worse than finetuning by 3.7% on MAE and outperforms finetuning by 2.3% on RMSE. However, Replay outperforms the finetuning by 12.9% on MAE and 3.6% on RMSE. Overall, Replay based method performs better in both indoor and outdoor scenarios, while the regularization methods do not seem to consistently outperform simple finetuning to a significant degree. There is one specific case when training VOICED model on waymo dataset where EWC and LWF performs much worse than Replay (i.e. Replay outperforms EWC by 72% and LWF by 84%).

Qualitative. For our model inversion method, we currently have qualitative results that show the difference in retrieval quality between baselines and continual learning methods. Figure 1 shows inversion results from KBnet models that have been pretrained on NYUv2 and finetuned on VOID, where the replay method outperforms the other continual learning methods, improving the finetuned model by 11.57%. As expected, the NYUv2 pretrained model is able to retrieve the 2D structure of the scene with higher fidelity than all of the models which have been trained on VOID afterwards; whereas the VOID model is unable to retrieve the image at all because it has never been trained on it. In line with the

quantitative results in Table V, we observe that the replay method can retrieve clearer object boundaries (e.g. the bottom of the vanity in the bottom right bounding box) and smoother surfaces (e.g. the wall in the top left bounding box).

VI. DISCUSSION

To the best of our knowledge, this is the first study to apply continual learning methods to the problem of depth completion. By establishing a benchmark for continual depth completion across indoor and outdoor datasets, this paper sets the foundation for future work in extending continual learning to more complex, multi-modal depth estimation problems. We hope that this contribution will motivate further research into more effective strategies to combat catastrophic forgetting in depth completion and related 3D tasks.

REFERENCES

- [1] R. M. French, “Catastrophic forgetting in connectionist networks,” *Trends in cognitive sciences*, vol. 3, no. 4, pp. 128–135, 1999.
- [2] M. McCloskey and N. J. Cohen, “Catastrophic interference in connectionist networks: the sequential learning problem,” in *Psychology of learning and motivation*. Elsevier, 1989, vol. 24, pp. 109–165.
- [3] S. Thrun, “Is learning the n -th thing any easier than learning the first?” *Advances in neural information processing systems*, vol. 8, 1995.
- [4] R. Ratcliff, “Connectionist models of recognition memory: constraints imposed by learning and forgetting functions.” *Psychological review*, vol. 97, no. 2, p. 285, 1990.
- [5] A. Wong and S. Soatto, “Unsupervised depth completion with calibrated backprojection layers,” in *Proceedings of the IEEE/CVF International Conference on Computer Vision*, 2021, pp. 12 747–12 756.
- [6] A. Wong, S. Cicek, and S. Soatto, “Learning topology from synthetic data for unsupervised depth completion,” *IEEE Robotics and Automation Letters*, vol. 6, no. 2, pp. 1495–1502, 2021.
- [7] A. Wong, X. Fei, S. Tsuei, and S. Soatto, “Unsupervised depth completion from visual inertial odometry,” *IEEE Robotics and Automation Letters*, vol. 5, no. 2, pp. 1899–1906, 2020.
- [8] J. Kirkpatrick, R. Pascanu, N. Rabinowitz, J. Veness, G. Desjardins, A. A. Rusu, K. Milan, J. Quan, T. Ramalho, A. Grabska-Barwinska, *et al.*, “Overcoming catastrophic forgetting in neural networks.” *Proceedings of the national academy of sciences*, vol. 114, no. 13, pp. 3521–3526, 2017.

[9] Z. Li and D. Hoiem, “Learning without forgetting,” in *Proceedings of the IEEE conference on computer vision and pattern recognition*, 2017, pp. 5077–5086.

[10] D. Rolnick, A. Ahuja, J. Schwarz, T. Lillicrap, and G. Wayne, “Experience replay for continual learning,” *Advances in neural information processing systems*, vol. 32, 2019.

[11] N. Silberman, D. Hoiem, P. Kohli, and R. Fergus, “Indoor segmentation and support inference from rgbd images,” in *European conference on computer vision*. Springer, 2012, pp. 746–760.

[12] A. Dai, A. X. Chang, M. Savva, M. Halber, T. Funkhouser, and M. Nießner, “Scannet: Richly-annotated 3d reconstructions of indoor scenes,” in *Proceedings of the IEEE conference on computer vision and pattern recognition*, 2017, pp. 5828–5839.

[13] A. Geiger, P. Lenz, and R. Urtasun, “Are we ready for autonomous driving? the kitti vision benchmark suite,” in *2012 IEEE Conference on Computer Vision and Pattern Recognition*. IEEE, 2012, pp. 3354–3361.

[14] P. Sun, H. Kretzschmar, X. Dotiwalla, A. Chouard, V. Patnaik, P. Tsui, J. Guo, Y. Zhou, Y. Chai, B. Caine, *et al.*, “Scalability in perception for autonomous driving: Waymo open dataset,” in *Proceedings of the IEEE/CVF Conference on Computer Vision and Pattern Recognition*, 2020, pp. 2446–2454.

[15] A. Gaidon, Q. Wang, Y. Cabon, and E. Vig, “Virtual kitti: An annotated virtual dataset for scene understanding,” in *Proceedings of the IEEE conference on computer vision and pattern recognition workshops*, 2016, pp. 28–37.

[16] F. Zenke, B. Poole, and S. Ganguli, “Continual learning through synaptic intelligence,” in *International conference on machine learning*. PMLR, 2017, pp. 3987–3995.

[17] R. Aljundi, F. Babiloni, M. Elhoseiny, M. Rohrbach, and T. Tuytelaars, “Memory aware synapses: Learning what (not) to forget,” in *Proceedings of the European conference on computer vision (ECCV)*, 2018, pp. 139–154.

[18] A. Chaudhry, P. K. Dokania, T. Ajanthan, and P. H. Torr, “Riemannian walk for incremental learning: Understanding forgetting and intransigence,” in *Proceedings of the European conference on computer vision (ECCV)*, 2018, pp. 532–547.

[19] G. Hinton, O. Vinyals, and J. Dean, “Distilling the knowledge in a neural network,” *arXiv preprint arXiv:1503.02531*, 2015.

[20] P. Dhar, R. V. Singh, K.-C. Peng, Z. Wu, and R. Chellappa, “Learning without memorizing,” in *Proceedings of the IEEE/CVF conference on computer vision and pattern recognition*, 2019, pp. 5138–5146.

[21] A. Rannen, R. Aljundi, M. B. Blaschko, and T. Tuytelaars, “Encoder based lifelong learning,” in *Proceedings of the IEEE international conference on computer vision*, 2017, pp. 1320–1328.

[22] K. Lee, K. Lee, J. Shin, and H. Lee, “Overcoming catastrophic forgetting with unlabeled data in the wild,” in *Proceedings of the IEEE/CVF International Conference on Computer Vision*, 2019, pp. 312–321.

[23] A. Rios and L. Itti, “Closed-loop memory gan for continual learning,” *arXiv preprint arXiv:1811.01146*, 2018.

[24] S. Zhai, Y. Cheng, W. Zhang, and F. Lu, “Lifelong gan: Continual learning for conditional image generation,” in *Proceedings of the IEEE/CVF International Conference on Computer Vision*, 2019, pp. 2759–2768.

[25] A. Douillard, M. Cord, C. Ollion, T. Robert, and E. Valle, “Podnet: Pooled outputs distillation for small-tasks incremental learning,” in *Proceedings of the IEEE/CVF Conference on Computer Vision and Pattern Recognition (CVPR)*, 2020, pp. 1951–1960.

[26] S. Hou, X. Pan, C. Change Loy, Z. Wang, and D. Lin, “Learning a unified classifier incrementally via rebalancing,” in *Proceedings of the IEEE/CVF Conference on Computer Vision and Pattern Recognition (CVPR)*, 2019, pp. 831–839.

[27] M. K. Titsias, J. Schwarz, A. G. d. G. Matthews, R. Pascanu, and Y. W. Teh, “Functional regularisation for continual learning with gaussian processes,” *arXiv preprint arXiv:1901.11356*, 2019.

[28] Y. Pan, F. Li, and W. K. Lee, “Continual deep learning by functional regularisation of memorable past,” *arXiv preprint arXiv:2007.15302*, 2020.

[29] C. V. Nguyen, Y. Li, T. D. Bui, and R. E. Turner, “Variational continual learning,” in *International Conference on Learning Representations*, 2018.

[30] A. Chaudhry, M. Rohrbach, M. Elhoseiny, T. Ajanthan, P. K. Dokania, P. H. Torr, and M. Ranzato, “On tiny episodic memories in continual learning,” *arXiv preprint arXiv:1902.10486*, 2019.

[31] M. Riemer, I. Cases, R. Ajemian, M. Liu, I. Rish, Y. Tu, and G. Tesauro, “Learning to learn without forgetting by maximizing transfer and minimizing interference,” *arXiv preprint arXiv:1810.11910*, 2018.

[32] J. S. Vitter, “Random sampling with a reservoir,” *ACM Transactions on Mathematical Software (TOMS)*, vol. 11, no. 1, pp. 37–57, 1985.

[33] D. Lopez-Paz and M. Ranzato, “Gradient episodic memory for continual learning,” *Advances in neural information processing systems*, vol. 30, 2017.

[34] S.-A. Rebiffé, A. Kolesnikov, G. Sperl, and C. H. Lampert, “icarl: Incremental classifier and representation learning,” in *Proceedings of the IEEE conference on Computer Vision and Pattern Recognition*, 2017, pp. 2001–2010.

[35] H. Shin, J. K. Lee, J. Kim, and J. Kim, “Continual learning with deep generative replay,” *Advances in neural information processing systems*, vol. 30, 2017.

[36] M. Riemer, T. Klinger, D. Bouneffouf, and M. Franceschini, “Scalable recollections for continual lifelong learning,” in *Proceedings of the AAAI conference on artificial intelligence*, vol. 33, no. 01, 2019, pp. 1352–1359.

[37] M. Rostami, S. Kolouri, and P. K. Pilly, “Complementary learning for overcoming catastrophic forgetting using experience replay,” *arXiv preprint arXiv:1903.04566*, 2019.

[38] B. Pfülb, A. Gepperth, and B. Bagus, “Continual learning with fully probabilistic models,” *arXiv preprint arXiv:2104.09240*, 2021.

[39] R. Kemker and C. Kanan, “Fearnnet: Brain-inspired model for incremental learning,” *arXiv preprint arXiv:1711.10563*, 2017.

[40] S. Gopalakrishnan, P. R. Singh, H. Fayek, S. Ramasamy, and A. Ambikapathi, “Knowledge capture and replay for continual learning,” in *Proceedings of the IEEE/CVF winter conference on applications of computer vision*, 2022, pp. 10–18.

[41] A. Ayub and A. R. Wagner, “Eec: Learning to encode and regenerate images for continual learning,” *arXiv preprint arXiv:2101.04904*, 2021.

[42] O. Ostapenko, M. Puscas, T. Klein, P. Jahnichen, and M. Nabi, “Learning to remember: A synaptic plasticity driven framework for continual learning,” in *Proceedings of the IEEE/CVF conference on computer vision and pattern recognition*, 2019, pp. 11321–11329.

[43] Y. X. Wu, L. Herranz, X. Liu, J. van de Weijer, B. Raducanu, and T. Tuytelaars, “Memory replay gans: Learning to generate new categories without forgetting,” in *Proceedings of the 32nd International Conference on Neural Information Processing Systems*, 2018, pp. 5967–5977.

[44] K. Zhu, W. Zhai, Y. Cao, J. Luo, and Z.-J. Zha, “Self-sustaining representation expansion for non-exemplar class-incremental learning,” in *Proceedings of the IEEE/CVF Conference on Computer Vision and Pattern Recognition*, 2022, pp. 9296–9305.

[45] X. Liu, C. Wu, M. Menta, L. Herranz, B. Raducanu, A. D. Bagdanov, S. Jui, and J. v. de Weijer, “Generative feature replay for class-incremental learning,” in *Proceedings of the IEEE/CVF Conference on Computer Vision and Pattern Recognition Workshops*, 2020, pp. 226–227.

[46] A. Iscen, J. Zhang, S. Lazebnik, and C. Schmid, “Memory-efficient incremental learning through feature adaptation,” in *Computer Vision–ECCV 2020: 16th European Conference, Glasgow, UK, August 23–28, 2020, Proceedings, Part XVI 16*. Springer, 2020, pp. 699–715.

[47] E. Belouadah and A. Popescu, “Il2m: Class incremental learning with dual memory,” in *Proceedings of the IEEE/CVF international conference on computer vision*, 2019, pp. 583–592.

[48] A. Douillard, A. Rame, G. Couairon, and M. Cord, “Dytox: Transformers for continual learning with dynamic token expansion,” in *Proceedings of the IEEE conference on computer vision and pattern recognition workshops*, 2022, pp. 9285–9295.

[49] J. Wang, H. He, M. B. A. McDermott, and P. Szolovits, “Learning to prompt for continual learning,” in *Proceedings of the IEEE/CVF Conference on Computer Vision and Pattern Recognition (CVPR)*, 2022, pp. 139–149.

[50] Z. Wang, Z. Zhan, L. Qi, J. Zhang, K. Chen, B. Liu, J. Peng, and T. Zhang, “Continual learning with lifelong vision transformer,” *Proceedings of the IEEE/CVF Conference on Computer Vision and Pattern Recognition (CVPR)*, pp. 10893–10903, 2022.

[51] H. Chawla, A. Varma, E. Arani, and B. Zonooz, “Continual learning of unsupervised monocular depth from videos,” in *Proceedings of the IEEE/CVF Winter Conference on Applications of Computer Vision*, 2024, pp. 8419–8429.

[52] N. Vödisch, K. Petek, W. Burgard, and A. Valada, “Codeps: Online

continual learning for depth estimation and panoptic segmentation,” *arXiv preprint arXiv:2303.10147*, 2023.

[53] H. Xu and J. Zhang, “Aanet: Adaptive aggregation network for efficient stereo matching,” in *Proceedings of the IEEE/CVF Conference on Computer Vision and Pattern Recognition*, 2020, pp. 1959–1968.

[54] Z. Berger, P. Agrawal, T. Y. Liu, S. Soatto, and A. Wong, “Stereoscopic universal perturbations across different architectures and datasets,” in *Proceedings of the IEEE/CVF Conference on Computer Vision and Pattern Recognition*, 2022, pp. 15 180–15 190.

[55] A. Wong, M. Mundhra, and S. Soatto, “Stereopagnosia: Fooling stereo networks with adversarial perturbations,” in *Proceedings of the AAAI Conference on Artificial Intelligence*, vol. 35, 2021, pp. 2879–2888.

[56] F. Wang, S. Galliani, C. Vogel, P. Speciale, and M. Pollefeys, “Patchmatchnet: Learned multi-view patchmatch stereo,” in *Proceedings of the IEEE/CVF Conference on Computer Vision and Pattern Recognition*, 2021, pp. 14 194–14 203.

[57] C. Godard, O. M. Aodha, and G. J. Brostow, “Unsupervised monocular depth estimation with left-right consistency,” in *Proceedings of the IEEE Conference on Computer Vision and Pattern Recognition (CVPR)*, 2017, pp. 270–279.

[58] X. Fei, A. Wong, and S. Soatto, “Geo-supervised visual depth prediction,” *IEEE Robotics and Automation Letters*, vol. 4, no. 2, pp. 1661–1668, 2019.

[59] A. Wong and S. Soatto, “Bilateral cyclic constraint and adaptive regularization for unsupervised monocular depth prediction,” in *Proceedings of the IEEE/CVF Conference on Computer Vision and Pattern Recognition*, 2019, pp. 5644–5653.

[60] R. Upadhyay, H. Zhang, Y. Ba, E. Yang, B. Gella, S. Jiang, A. Wong, and A. Kadambi, “Enhancing diffusion models with 3d perspective geometry constraints,” *ACM Transactions on Graphics (TOG)*, vol. 42, no. 6, pp. 1–15, 2023.

[61] N. Zhang, F. Nex, G. Vosselman, and N. Kerle, “Lite-mono: A lightweight cnn and transformer architecture for self-supervised monocular depth estimation,” in *Proceedings of the IEEE/CVF Conference on Computer Vision and Pattern Recognition*, 2023, pp. 18 537–18 546.

[62] Y. Zhang, M. Poggi, F. Tosi, X. Guo, Z. Zhu, G. Huang, and S. Mattoccia, “Monovit: Self-supervised monocular depth estimation with a vision transformer,” in *Proceedings of the IEEE/CVF Conference on Computer Vision and Pattern Recognition*, 2023, pp. 9708–9719.

[63] Z. Zeng, Y. Wu, H. Park, D. Wang, F. Yang, S. Soatto, D. Lao, B.-W. Hong, and A. Wong, “Rsa: Resolving scale ambiguities in monocular depth estimators through language descriptions,” *Advances in neural information processing systems*, 2024.

[64] Z. Zeng, D. Wang, F. Yang, H. Park, S. Soatto, D. Lao, and A. Wong, “Worddepth: Variational language prior for monocular depth estimation,” in *Proceedings of the IEEE/CVF Conference on Computer Vision and Pattern Recognition*, 2024, pp. 9708–9719.

[65] M. Jaritz, R. De Charette, E. Wirbel, X. Perrotton, and F. Nashashibi, “Sparse and dense data with cnns: Depth completion and semantic segmentation,” in *2018 International Conference on 3D Vision (3DV)*. IEEE, 2018, pp. 52–60.

[66] V. Ezhov, H. Park, Z. Zhang, R. Upadhyay, H. Zhang, C. C. Chandrappa, A. Kadambi, Y. Ba, J. Dorsey, and A. Wong, “All-day depth completion,” in *2023 IEEE/RSJ International Conference on Intelligent Robots and Systems (IROS)*. IEEE, 2024.

[67] A. D. Singh, Y. Ba, A. Sarker, H. Zhang, A. Kadambi, S. Soatto, M. Srivastava, and A. Wong, “Depth estimation from camera image and mmwave radar point cloud,” in *Proceedings of the IEEE/CVF Conference on Computer Vision and Pattern Recognition*, 2023, pp. 9275–9285.

[68] Y. Yang, A. Wong, and S. Soatto, “Dense depth posterior (ddp) from single image and sparse range,” in *Proceedings of the IEEE/CVF Conference on Computer Vision and Pattern Recognition*, 2019, pp. 3353–3362.

[69] T. Y. Liu, P. Agrawal, A. Chen, B.-W. Hong, and A. Wong, “Monitored distillation for positive congruent depth completion,” in *Computer Vision–ECCV 2022: 17th European Conference, Tel Aviv, Israel, October 23–27, 2022, Proceedings, Part II*. Springer, 2022, pp. 35–53.

[70] Y. Wu, T. Y. Liu, H. Park, S. Soatto, D. Lao, and A. Wong, “Augundo: Scaling up augmentations for monocular depth completion and estimation,” in *European Conference on Computer Vision*. Springer, 2024.

[71] H. Park, A. Gupta, and A. Wong, “Test-time adaptation for depth completion,” in *Proceedings of the IEEE/CVF Conference on Computer Vision and Pattern Recognition*, 2024, pp. 20 519–20 529.

[72] M. Hu, S. Wang, B. Li, S. Ning, L. Fan, and X. Gong, “Penet: Towards precise and efficient image guided depth completion,” in *2021 IEEE International Conference on Robotics and Automation (ICRA)*. IEEE, 2021, pp. 13 656–13 662.

[73] A. Li, Z. Yuan, Y. Ling, W. Chi, C. Zhang, et al., “A multi-scale guided cascade hourglass network for depth completion,” in *Proceedings of the IEEE/CVF Winter Conference on Applications of Computer Vision*, 2020, pp. 32–40.

[74] J. Park, K. Joo, Z. Hu, C. Liu, and I.-S. Kweon, “Non-local spatial propagation network for depth completion,” in *European Conference on Computer Vision (ECCV)*, 2020, pp. 120–136.

[75] A. Eldesokey, M. Felsberg, K. Holmquist, and M. Persson, “Uncertainty-aware cnns for depth completion: Uncertainty from beginning to end,” in *Proceedings of the IEEE/CVF Conference on Computer Vision and Pattern Recognition (CVPR)*, 2020, pp. 12 014–12 023.

[76] W. Van Gansbeke, D. Neven, B. De Brabandere, and L. Van Gool, “Sparse and noisy lidar completion with rgb guidance and uncertainty,” in *2019 16th International Conference on Machine Vision Applications (MVA)*. IEEE, 2019, pp. 1–6.

[77] Y. Zhang and T. Funkhouser, “Deep depth completion of a single rgb-d image,” in *Proceedings of the IEEE Conference on Computer Vision and Pattern Recognition*, 2018, pp. 175–185.

[78] Y. Zhang, X. Guo, M. Poggi, Z. Zhu, G. Huang, and S. Mattoccia, “Completionformer: Depth completion with convolutions and vision transformers,” in *Proceedings of the IEEE/CVF Conference on Computer Vision and Pattern Recognition*, 2023, pp. 18 527–18 536.

[79] Z. Yu, Z. Sheng, Z. Zhou, L. Luo, S. Cao, H. Gu, H. Zhang, and H. Shen, “Aggregating feature point cloud for depth completion,” in *Proceedings of the IEEE/CVF International Conference on Computer Vision*, 2023, pp. 8732–8743.

[80] F. Ma, G. Cavalheiro, and S. Karaman, “Self-supervised sparse-to-dense: Self-supervised depth completion from lidar and monocular camera,” in *2019 International Conference on Robotics and Automation (ICRA)*. IEEE, 2019, pp. 3288–3295.

[81] S. S. Shivakumar, T. Nguyen, I. D. Miller, S. W. Chen, V. Kumar, and C. J. Taylor, “Dfusenet: Deep fusion of rgb and sparse depth information for image guided dense depth completion,” in *2019 IEEE Intelligent Transportation Systems Conference (ITSC)*. IEEE, 2019, pp. 13–20.

[82] A. Wong, X. Fei, B.-W. Hong, and S. Soatto, “An adaptive framework for learning unsupervised depth completion,” *IEEE Robotics and Automation Letters*, vol. 6, no. 2, pp. 3120–3127, 2021.

[83] Z. Yan, K. Wang, X. Li, Z. Zhang, J. Li, and J. Yang, “Desnet: Decomposed scale-consistent network for unsupervised depth completion,” in *Proceedings of the AAAI Conference on Artificial Intelligence*, vol. 37, no. 3, 2023, pp. 3109–3117.

[84] V. Lepetit, F. Moreno-Noguer, and P. Fua, “Epnp: An accurate o (n) solution to the pnp problem,” *International journal of computer vision*, vol. 81, no. 2, p. 155, 2009.

[85] M. A. Fischler and R. C. Bolles, “Random sample consensus: a paradigm for model fitting with applications to image analysis and automated cartography,” *Communications of the ACM*, vol. 24, no. 6, pp. 381–395, 1981.

[86] A. Lopez-Rodriguez, B. Busam, and K. Mikolajczyk, “Project to adapt: Domain adaptation for depth completion from noisy and sparse sensor data,” in *Proceedings of the Asian Conference on Computer Vision (ACCV)*, 2020.

[87] J. Jeon, H. Lim, D. U. Seo, and H. Myung, “Struct-mdc: Mesh-refined unsupervised depth completion leveraging structural regularities from visual slam,” in *IEEE Robotics and Automation Letters (RA-L)*, vol. 7, no. 3, 2022, pp. 6391–6398.